Self-assembled synthesis of 3D $Cu(In_{1-x}Ga_x)Se_2$ nanoarrays by one-step electroless deposition into ordered AAO template

2014 Nanotechnology 25 295601

(http://iopscience.iop.org/0957-4484/25/29/295601)

IOP Publishing Nanotechnology
Nanotechnology **25** (2014) 295601 (8pp) doi:10.1088/0957-4484/25/29/295601

Self-assembled synthesis of 3D Cu($In_{1-x}Ga_x$)Se_2 nanoarrays by one-step electroless deposition into ordered AAO template

Bin Zhang[1], Tao Zhou[2], Maojun Zheng[1], Zuzhou Xiong[1], Changqing Zhu[1], Hong Li[1], Faze Wang[1], Li Ma[3] and Wenzhong Shen[1]

[1] Key Laboratory of Artificial Structures and Quantum Control (Ministry of Education), Department of Physics and Astronomy, Shanghai Jiao Tong University, Shanghai, 200240, People's Republic of China
[2] School of Mathematics and Physics, Shanghai University of Electric Power, Shanghai, 200090, People's Republic of China
[3] School of Chemistry and Chemical Technology, Shanghai Jiao Tong University, Shanghai, 200240, People's Republic of China

E-mail: taozhou@shiep.edu.cn and mjzheng@sjtu.edu.cn

Received 25 February 2014, revised 28 April 2014
Accepted for publication 27 May 2014
Published 1 July 2014

Abstract

Quaternary nanostructured Cu($In_{1-x}Ga_x$)Se_2 (CIGS) arrays were successfully fabricated via a novel and simple solution-based protocol on the electroless deposition method, using a flexible, highly ordered anodic aluminium oxide (AAO) substrate. This method does not require electric power, complicated sensitization processes, or complexing agents, but provides nearly 100% pore fill factor to AAO templates. The field emission scanning electron microscopy (FE-SEM) images show that we obtained uniformly three-dimensional nanostructured CIGS arrays, and we can tailor the diameter and wall thicknesses of the nanostructure by adjusting the pore diameter of the AAO and metal Mo layer. Their chemical composition was determined by energy-dispersive spectroscopy analysis, which is very close to the stoichiometric value. The Raman spectroscopy, x-ray diffraction (XRD) pattern, and transmission electron microscopy (TEM) further confirm the formation of nanostructured CIGS with prominent chalcopyrite structure. The nanostructured CIGS arrays can support the design of low-cost, highlight-trapping, and enhanced carrier collection nanostructured solar cells.

Keywords: CIGS, nanostructure arrays, galvanic displacement method, self-assembly

(Some figures may appear in colour only in the online journal)

1. Introduction

Chalcopyrite quaternary Cu($In_{1-x}Ga_x$)Se_2 (CIGS) compound semiconductors are considered to the most promising absorber materials for thin film photovoltaic applications because they have high absorption coefficients of visible light up to about 10^5 cm^{-1}, the ability to undergo band gap engineering through alloy formation, and long-term reliable optoelectronic stability [1–3]. To date, thin film photovoltaic devices based on chalcopyrite CIGS absorber layers show excellent light-to-power conversion efficiencies of about 20.4% [4]. However, the best performance of CIGS absorber film was produced by a three-stage co-evaporation process, which can severely hinder the diffusion of this device because of the high-cost vacuum deposition techniques and low material utilization. Therefore, these factors have led to the continued development and investigation of wide novel materials processing and device structures for enabling acceptable efficiencies [5–7].

On the one hand, the low-cost and convenient non-vacuum-based approaches, such as chalcogenide-hydrazine complex precursors [8, 9], sol-gel spin coating process [10], electrodeposition [11–15], and nanoparticle-based inks [16–19], generate significant research interest as potential alternatives. Among the different non-vacuum-based methods, the most intensely investigated and striking strategy may be the solution-based methods. Compared with vacuum-based deposition techniques, the solution-based methods have many advantages, such as low instrumental and material costs, high throughput, controllability of chemical composition, efficient utilization of raw materials, and feasibility in making large-area film [20, 21]. The hydrazine solution processed solar cells have achieved, to date, 15.2% power-conversion efficiency [22]. However, hydrazine is highly toxic and must be handled with appropriate protective equipment to prevent contact with either the vapors or liquid.

On the other hand, nanostructure materials have received ever-increasing interest over the past several decades owing to their remarkable properties and intriguing applications in many areas such as catalysis [23], superhydrophobic surfaces [24], semiconductors [25], biosensors [26], and solar cells [27–29]. Additionally, diverse parameters of nanoporous anodic aluminium oxide (AAO) can be easily prepared by adjusting anodizing potential and electrolytes. Accordingly, high-ordered AAO is considered to be one of the most suitable host or template materials for nanomaterial fabrication [30, 31].

In recent years, we have also made many efforts to synthesize nanostructured absorber materials by simple, solution-based methods. In previous works, we have reported self- and directed-assembly of $CuInSe_2$ nanotubes and CIGS nanopores by highly ordered AAO templates [32, 33]. In the present work, we report a novel nonhydrazine solution process employing a direct electroless deposition to prepare CIGS nanostructured arrays. It is important that we can tailor the morphology of the nanostructure arrays by adjusting some physical parameters, including the pore diameter size of the AAO template and the metal Mo layer.

2. Experimental setup

2.1. Preparation of anodic aluminum oxide template

It is widely recognized that ideally ordered AAO can be prepared through mild anodization and hard anodization [34, 35]. In this work, AAO was fabricated using two previously published procedures [36, 37]. First, high-purity circular aluminum sheets (99.999%, 2.5 cm in diameter, 0.25 mm thick) were used as starting specimens. Then, the specimens were degreased in acetone, washed by deionized water, and electropolished at a constant voltage, 10 V, in a 1:4 volume mixture of perchloric acid and ethanol at room temperature. The first-step anodization was performed in a 0.25 M phosphoric acid electrolyte solution at the potential 195 V for 100 s and −4 °C (or 0.3 M oxalic acid, 40 V, 2 h, 10 °C), with vigorous magnetic stirring. A power cooling system and a large electrolysis cell (2 L) were used to maintain the low temperature required for high-field anodization. Then, the first anodization specimens were immersed in a mixture of 6.0 wt% phosphoric acid and 1.8 wt% chromic acid at 60 °C for 4 h to remove the alumina layers with an orderless surface. The well-ordered concave patterns on the aluminum foil acted as self-assembled masks for the second anodization. The second anodization was performed under the same conditions as the first. Finally, after removing the remaining aluminum on the back side in a 1:3 volume mixture of hydrochloric acid and saturated copper sulfate solution at room temperature, pore openings were created in a 5 wt% phosphoric acid solution at 45 °C for 60 min Most importantly, it should be noted that a fraction of Al foil surrounding the fabrication of the porous AAO template was not anodized. Moreover, the remaining Al played a key role in the deposition process. The morphology of the specimens was investigated by a field-emission scanning electron microscope (FE-SEM; FEI Sirion 200).

2.2. Sputtering molybdenum back electrode

A Mo layer was deposited on the back side of the AAO by magnetron sputtering in Ar gas at a pressure of 8 mTorr at room temperature. The Mo films were sputtered from a molybdenum target foil (diameter: 75 mm, thickness: 5 cm, purity: 99.999%). First, the vacuum chamber was evacuated to a base pressure of 10^{-4} pa. Then the power supply was turned on and the sputtering power adjusted to 50 w. Through changing the sputtering time, we can obtain diverse pore diameters in the nanopore Mo films on the AAO in order to control the wall thickness of the nanostructures.

2.3. Electroless deposition CIGS

The nonhydrazine solution for synthesis of CIGS nanostructured arrays was a mixture. The molar concentrations of the individual salts in the deposition solution were as follows: 2.5 mM $CuCl_2$, 7.5 mM $InCl_3$, 10 mM $GaCl_3$, and 5 mM H_2SeO_3. The pH value of the mixture solution was adjusted to 2.2 by 5 M NaOH buffer solution. The electroless deposition time was precisely controlled to obtain 1–2 μm high arrays. Following electroless deposition, the samples were soaked in deionized water and dried under a steady stream of nitrogen. Then, the as-prepared samples were annealed at 550 °C temperature with the heat in rate of 10 °C per min in a vacuum tube furnace for 30 min.

2.4. Characterization

The morphology of the as-prepared and annealed CIGS nanostructured arrays were observed by FE-SEM (FEI Sirion 200). The composition was investigated by an energy-dispersive x-ray spectrometer (EDS) system (Inca Oxford) attached to the FE-SEM. The Raman spectra were measured by an InVia-Reflex Micro-Raman spectroscopy system (Renishaw, English). A laser wavelength of 532 nm was used as the excitation source. The crystallographic structure was determined by x-ray diffraction (XRD; D8 DISCOVER x-ray

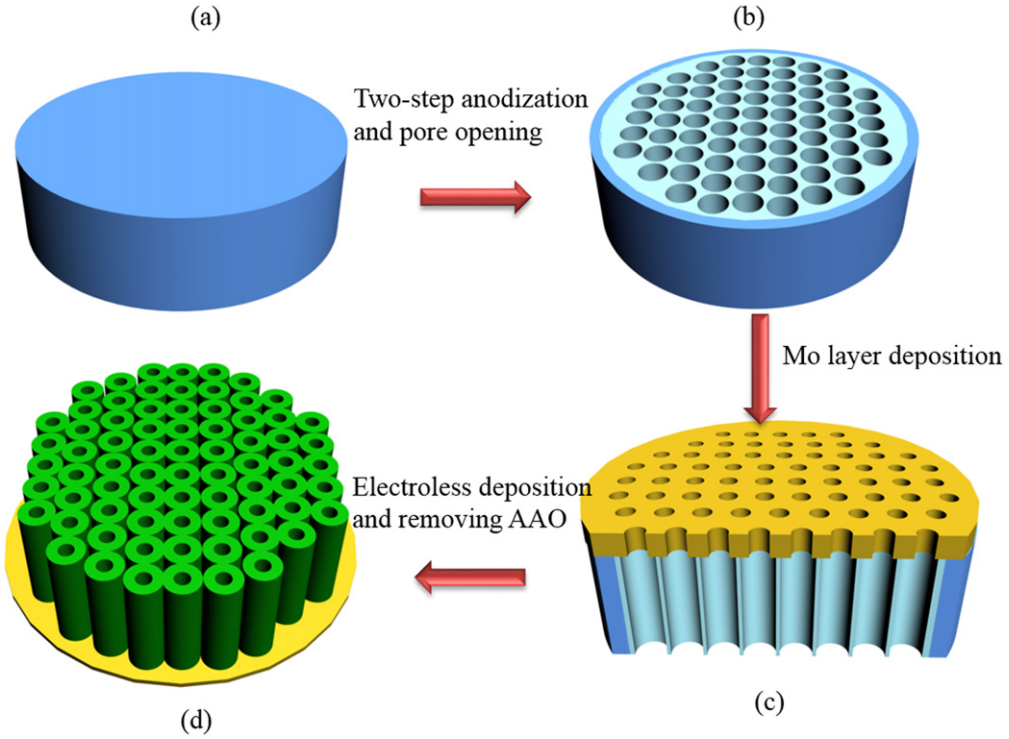

Figure 1. Schematic illustration of the fabrication process of the CIGS nanostructured arrays: (a) AI wafer, (b) through-hole AAO template with a narrow ring-shaped Al foil fabricated via two-step anodization and hole-opening, (c) Mo layer deposited on AAO template via sputtering and its cross section, and (d) as-prepared CIGS nanostructured arrays after removing the AAO template.

diffractometer, Bruker, Germany) with Cu K α radiation ($\lambda = 1.54$ Å). Transmission electron microscopy (TEM) images, and the corresponding selected area electron diffraction patterns, were taken on a JEOL JEM2100F.

3. Results and discussion

Figure 1 shows a schematic diagram of the fabrication process of CIGS nanostratured arrays. After Al wafers were degreased, washed, and electropolished, a through-hole AAO template with a narrow, ring-shaped Al foil was fabricated via two-step anodization and hole-opening. Then the Mo-coated AAO template prepared via sputtering was put into the mixed solution consisting of 2.5 mM $CuCl_2$, 7.5 mM $InCl_3$, 10 mM $GaCl_3$, and 5 mM H_2SeO_3, in which a galvanic displacement reaction occurred. The formation process of CIGS nanostructured arrays can be explained by galvanic displacement method. The growth mechanism was reported in detail in our previous work [32]. When the pH value of the solution is about 2.2, the following galvanic displacement reaction will occur:

$$3Cu^{2+}(aq) + 3(1 - x)In^{3+}(aq) + 3xGa^{3+}(aq) + 6SeO_3^{2+}(aq) + 13Al^0(s) + 36H^+(aq) \rightarrow 3CuIn_{1-x}Ga_xSe_2(s) + 13Al^{3+}(aq) + 18H_2O.$$

The morphology of the as-prepared CIGS nanostructured arrays depends on the AAO and the Mo layer, as the CIGS was grown on the Mo layer and confined in channels of the AAO template. On one hand, we used high-field and low-field to obtain different AAO pore diameters. Figure 2 presents the SEM pictures of the as-prepared highly ordered AAO template. Figures 2(a) and (b) are the FE-SEM images of the top view and the cross-sectional view of the AAO template prepared by high-field anodization method; figures 2(c) and (d) were prepared by the low-field anodization method. The pore diameters of the AAO are about 200–275 nm and 75–120 nm, respectively, in images (b) and (d). By using the high-field and the low-field AAO, we can obtain different outside diameter CIGS arrays. On the other hand, we can control the sputtering time to obtain different pore diameter metal Mo layers, in order to gain various inside diameter CIGS arrays. The surface morphology of the deposition metal Mo layers on AAO with different sputtering times was displayed in figure 3. In figures 3(a)–(c), the sputtering time was 2 min, 4 min, and 12 min, respectively, on high-field AAO; the pore diameters of the obtained corresponding porous Mo layers were about 135 nm, 110 nm, and 57 nm on average. In figure 3(d), the deposition time was 5 min on the low-field AAO, and the Mo layer pore diameter was 19 nm.

Figure 4 presents the SEM images of the as-synthetized CIGS arrays with different morphology grown on different AAO templates (figures 4(a)–(d) are high-field AAOs, (e) and (f) are low-field AAOs) with different sputtering times of the Mo layer (figure 4(a) 2 min, (b) 4 min, (c) 12 min, (d) 18 min, (e) and (f) 5 min). Importantly, these CIGS arrays have nearly 100% pore-fill factor of the AAO templates. Figures 4(a)–(d) confirm that we have obtained different inside-pore-diameter CIGS arrays, ranging from 160 nm to 0 nm (in other words,

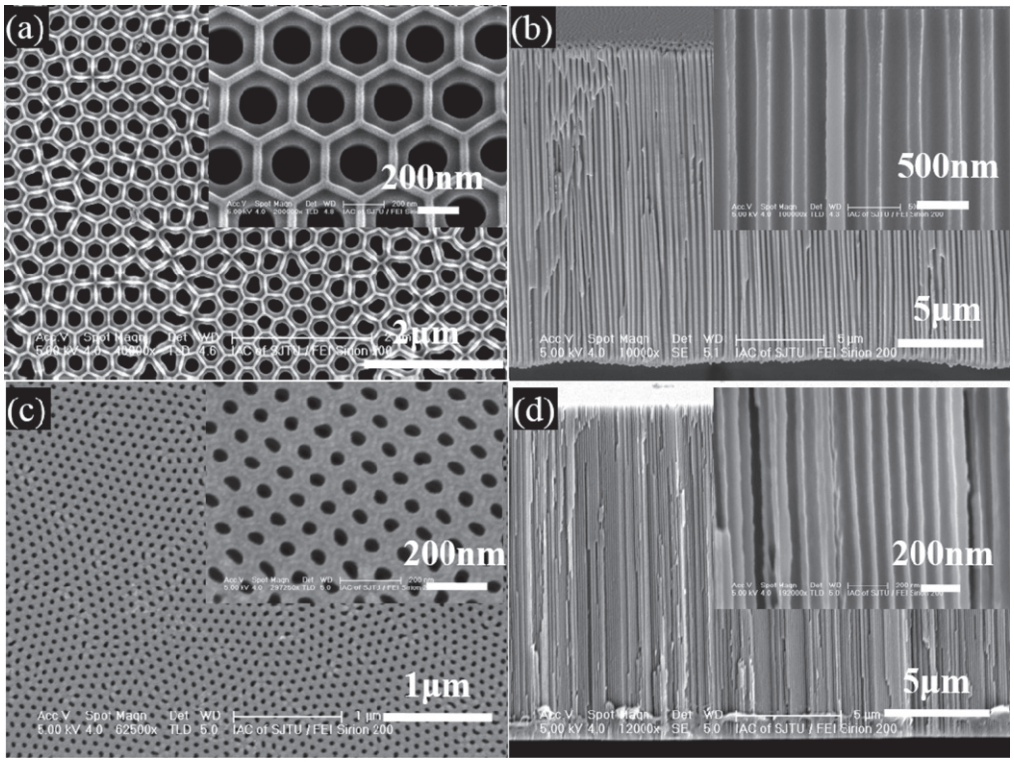

Figure 2. (a) FE-SEM images of highly ordered AAO template. (a) Top view and (b) cross-sectional view of the AAO template prepared by high-field anodization method. (c) Top view and (d) cross-sectional view of the AAO template prepared by low-field anodization method.

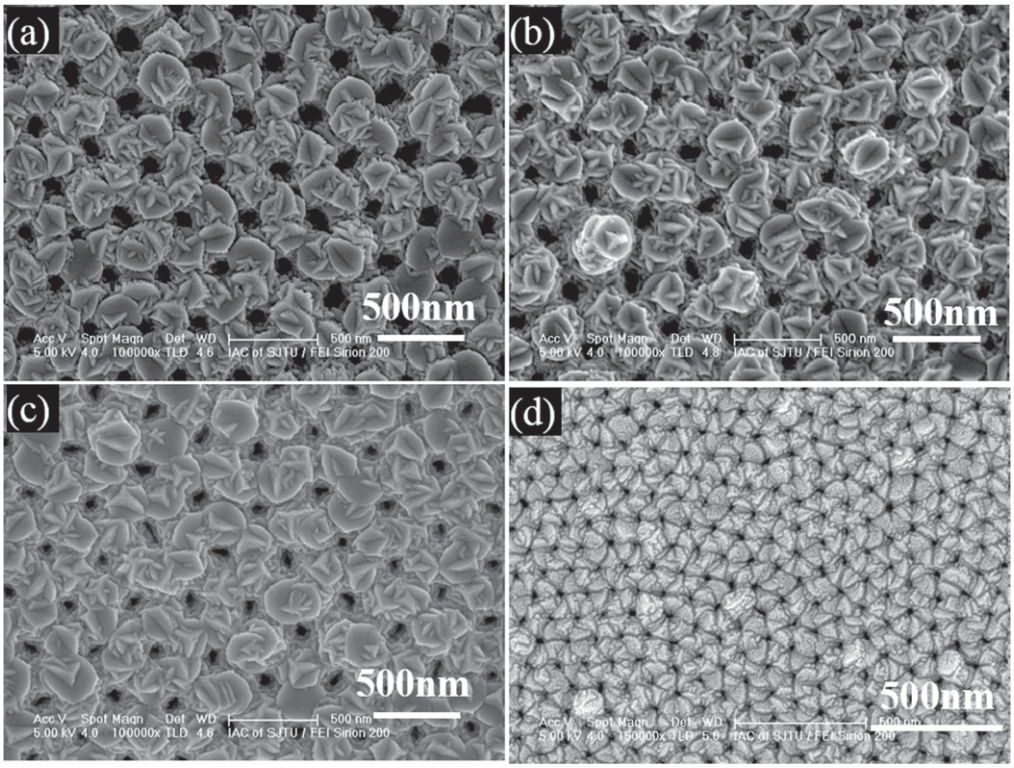

Figure 3. The surface morphology of the sputtering Mo layer with different sputtering times: (a) 2 min, (b) 4 min, (c) 12 min, (d) 5 min.

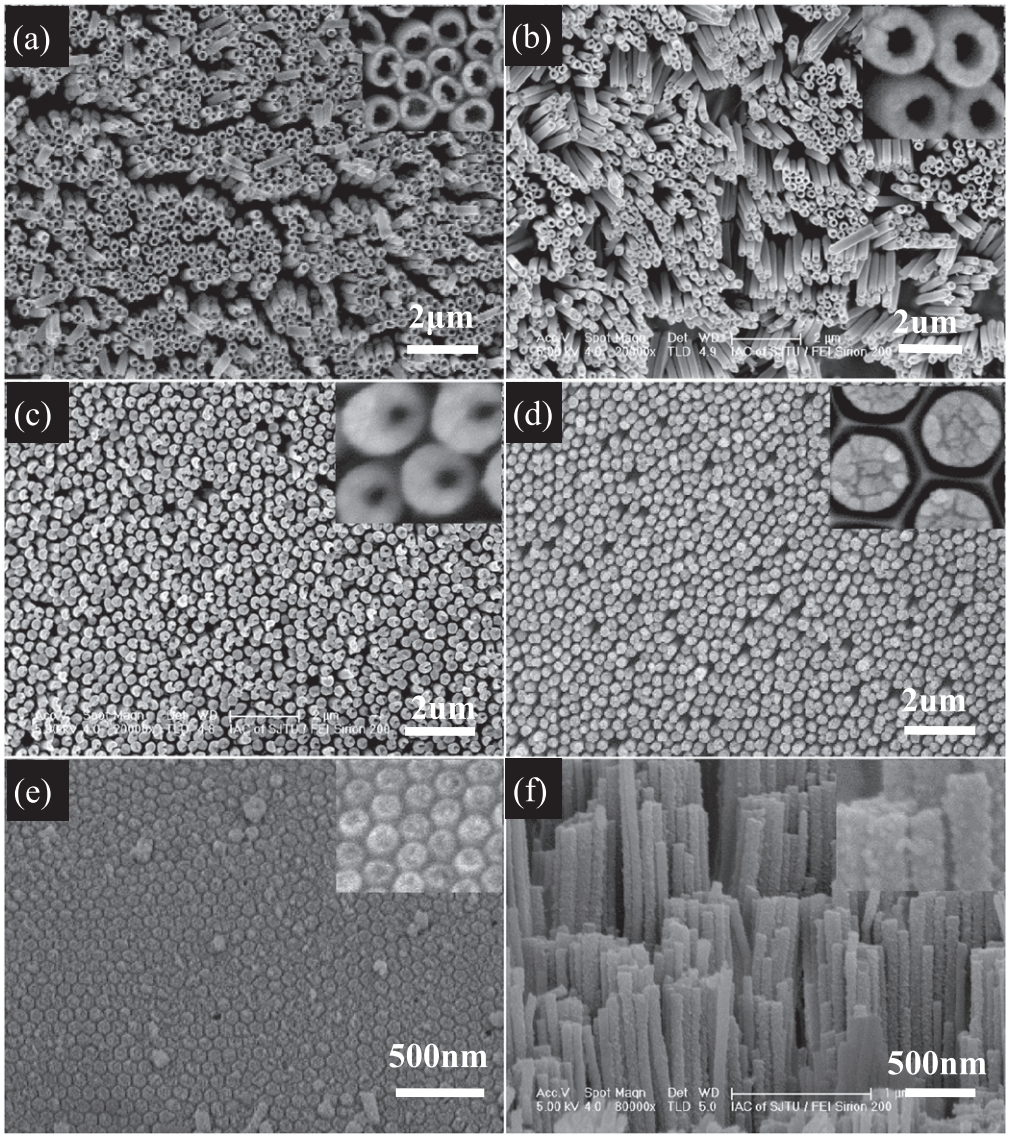

Figure 4. SEM images of the as-synthetized CIGS samples with different morphology grown on different AAO templates: (a)–(d) high-field template, (e) and (f) low-field template. The sputtering time of the MO layer: (a) 2 min, (b) 4 min, (c) 12 min, (d) 18 min, (e) and (f) 5 min.

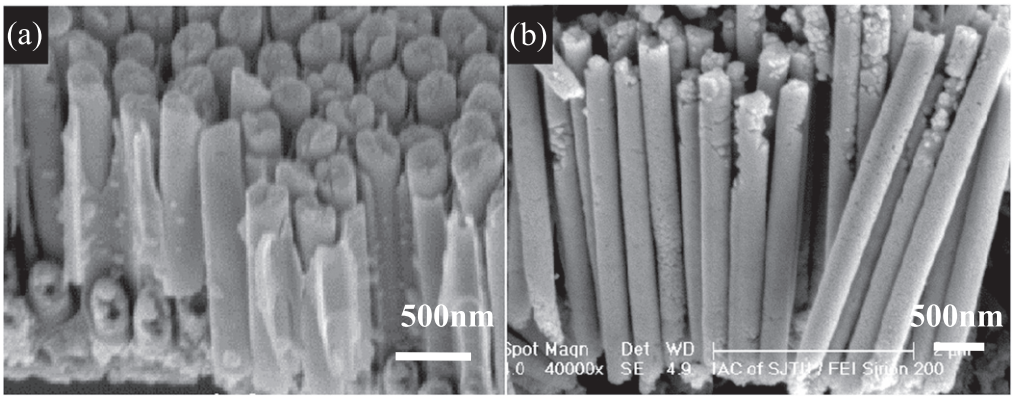

Figure 5. The cross-sectional picture of CIGS arrays grown for (a) 30 min and (b) 60 min.

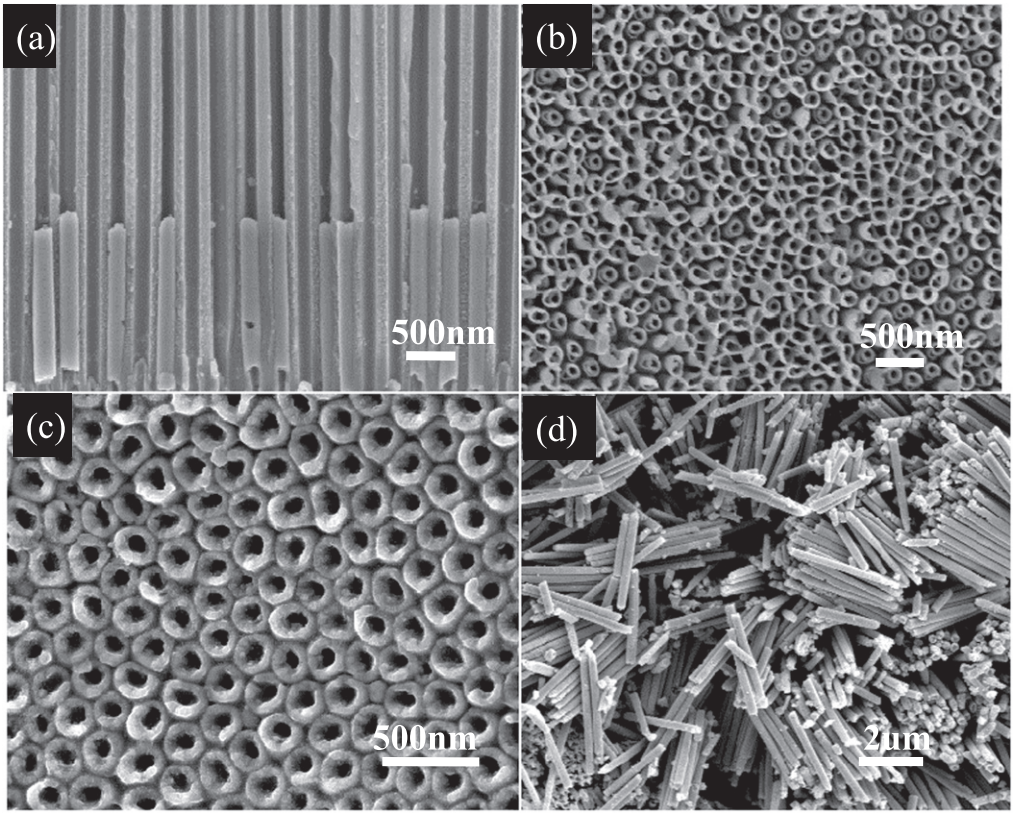

Figure 6. SEM images of the as-synthetized CIGS arrays with different removing template times: (a) 0 min, (b) 40 min, (c) 45 min, and (d) 50 min.

different wall thicknesses) by controlling the sputtering time of the metal Mo layer. Figures 4(d) and (e) illustrate that the outside pore diameter of CIGS arrays depended on whether the as-prepared AAO was high-field or low-field.

In addition, the length of the CIGS arrays can be changed by adjusting the growth time. The images in figures 5(a) and (b) were grown for 30 min and 60 min, respectively. Finally, we removed the AAO template using 5 wt% phosphoric acid solution. The different removing time can change the surrounding condition of the arrays (figures 6(a) and (b) embedding, (c) freestanding, and (d) separating). The images in figures 6(a)–(d) show the AAO with removing times at 0 min, 40 min, 45 min, and 50 min, respectively.

Their chemical compositions, which were very close to the stoichiometric value, were determined by energy-dispersive spectroscopy analysis. Figure 7 shows that the composition of the CIGS nanostructure arrays is 28.41:17.54:9.86:44.18. The controllability of composition is an important advantage in the fabrication of CIGS by solution process. This EDS mapping analysis displays a homogeneous distribution of the four elements Cu, In, Ga, and Se on the 2D-projected chemical maps of the nanostructure.

The Raman spectroscopy, XRD patterns, and TEM were further used to confirm the formation of nanostructured CIGS with a prominent expected chalcopyrite structure. Figure 8(a) presents the Raman spectrum of the as-synthesized CIGS. The strong peak centered at 170 cm^{-1} corresponds to the A_1 mode of the chalcopyrite CIGS. As figure 8(b) depicts, the

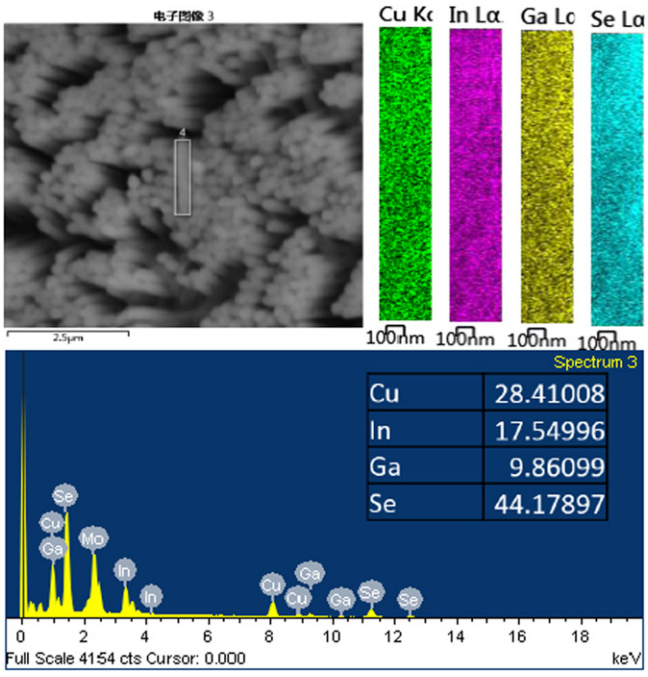

Figure 7. EDS mapping and EDS results of the CIGS nanostructure arrays.

XRD pattern of the CIGS array demonstrates (112), (220), (312), (400), (332), (424), and (512) diffraction peaks corresponding to expected 2θ positions, which indicate the formation of single-phase chalcopyrite CIGS without other

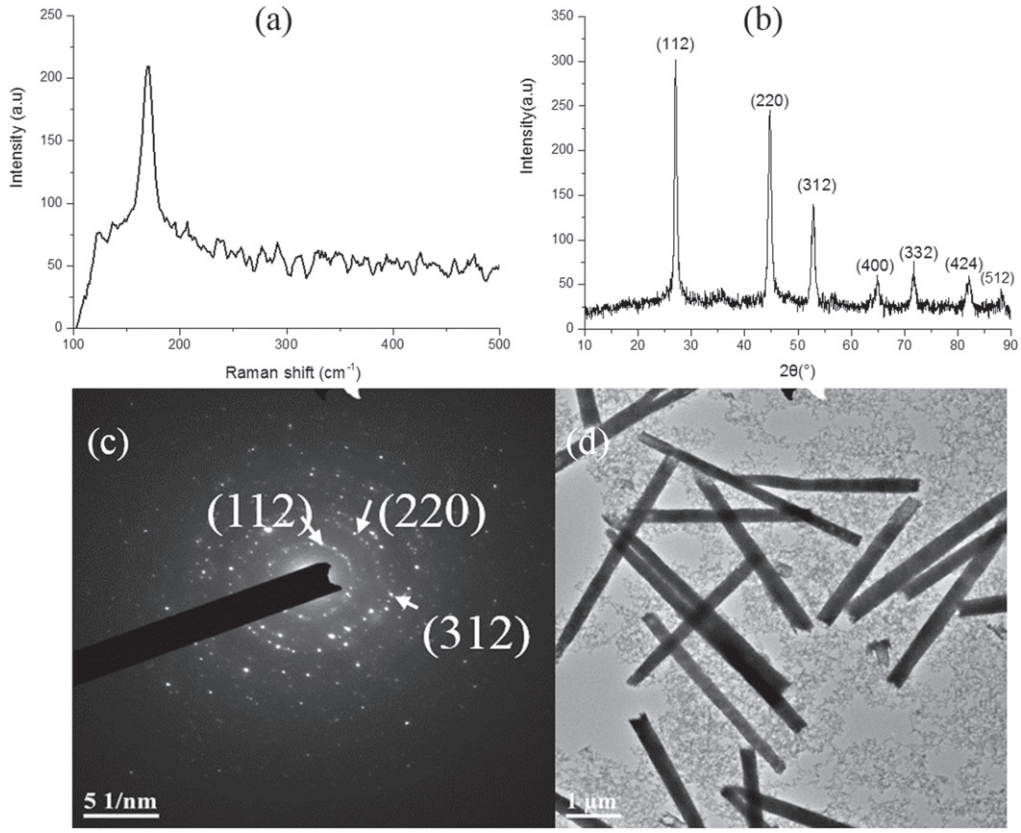

Figure 8. The characterization picture of the as-synthetized CIGS nanostructure arrays. (a) The Raman spectrum of the CIGS arrays, (b) the XRD patterns of the as-synthetized CIGS nanostructure arrays, (c) and (d) the TEM image and selected area electron diffraction pattern of the nanostructured CIGS.

impurity phases, according to the standard bulk crystal structure pattern of $CuIn_{0.7}Ga_{0.3}Se_2$(PDF 35–1102). In addition, figures 8(c) and (d) show TEM images of nanostructured CIGS. The chalcopyrite characteristic peaks such as (112), (220), and (312) show good agreement with the results of the XRD pattern. Therefore, the as-synthesized CIGS nanostructure array is qualified and available for absorber-layer fabrication.

4. Conclusions

In summary, a simple nonhydrazine solution-based electroless chemical deposition method has been developed for fabricating CIGS nanostructure arrays for the absorber layer of nanostructure solar cells. Compared with conventional electrodeposition techniques, this method does not require electric power, complicated sensitization processes, or complexing agents, but provides a nearly 100% pore-fill factor for AAO templates. Moreover, the AAO template and the Mo layer provide CIGS nanostructured arrays that are nanochannel-confined for growth. We demonstrated the fabrication of nanostructured CIGS arrays with diverse diameters and wall thicknesses by using different pore diameter AAO templates and metal Mo layers. The controllability and tunability of composition is an important advantage in the fabrication of CIGS by this solution process. The nanostructured CIGS arrays can support the design of low-cost, highlight-trapping, and enhanced carrier collection nanostructured solar cells. Moreover, we are using this method to fabricate nanostructured solar cells and synthesize other material nanostructured arrays, such as Cu_2ZnSnS_4.

Acknowledgments

We are grateful to X Wu for assistance with XRD. This work was supported by the National Major Basic Research Project of 2012CB934302, National 863 Program 2011AA050518, the Natural Science Foundation of China (grant Nos. 11174197 and 61234005).

References

[1] Anjun H, Yi Z, Wei S, Boyan L, Wei L and Yun S 2012 Structure, morphology and properties of thinned Cu(In, Ga)Se_2 films and solar cells *Semicond. Sci. Technol.* **27** 035022

[2] Contreras M A, Mansfield L M, Egaas B, Li J, Romero M, Noufi R, Rudiger-Voigt E and Mannstadt W 2012 Wide bandgap Cu(In, Ga)Se_2 solar cells with improved energy conversion efficiency *Prog. Photovolt. Res. Appl.* **20** 843–50

[3] Siebentritt S, Igalson M, Persson C and Lany S 2010 The electronic structure of chalcopyrites—bands, point defects and grain boundaries *Prog. Photovolt. Res. Appl.* **18** 390–410

[4] Chirilă A *et al* 2013 Potassium-induced surface modification of Cu(In, Ga)Se_2 thin films for high-efficiency solar cells *Nat. Mater.* **12** 1107–11

[5] Fan Z *et al* 2009 Three-dimensional nanopillar-array photovoltaics on low-cost and flexible substrates *Nat. Mater.* **8** 648–53

[6] Liao Y *et al* 2013 Non-antireflective scheme for efficiency enhancement of Cu(In, Ga)Se_2 nanotip array solar cells *ACS Nano* **7** 7318–29

[7] Liu C *et al* 2011 Large scale single-crystal Cu(In, Ga)Se_2 nanotip arrays for high efficiency solar cell *Nano Lett.* **11** 4443–8

[8] Bob B, Lei B, Chung C, Yang W, Hsu W, Duan H, Hou W W, Li S and Yang Y 2012 The development of hydrazine-processed Cu(In, Ga)(Se, S)$_2$ solar cells *Adv. Energy Mater.* **2** 504–22

[9] Liu W, Mitzi D B, Yuan M, Kellock A J, Chey S J and Gunawan O 2010 12% efficiency CuIn(Se, S)$_2$ photovoltaic device prepared using a hydrazine solution process *Chem. Mater.* **22** 1010–4

[10] Park J W, Choi Y W, Lee E, Joo O S, Yoon S and Min B K 2009 Synthesis of CIGS absorber layers via a paste coating *J. Crysta. Growth* **311** 2621–5

[11] Bhattacharya R N, Oh M and Kim Y 2012 CIGS-based solar cells prepared from electrodeposited precursor films *Sol. Energy Mater. Sol. Cells* **98** 198–202

[12] Chaure N B 2013 Electrodeposited $CuIn_{1-x}Ga_xSe_2$ thin films from non-aqueous medium for solar cell applications *J. Renew. Sustain. Ener.* **5** 031604

[13] Harati M, Jia J, Giffard K, Pellarin K, Hewson C, Love D A, Lau W M and Ding Z 2010 One-pot electrodeposition, characterization and photoactivity of stoichiometric copper indium gallium diselenide (CIGS) thin films for solar cells *Phys. Chem. Chem. Phys.* **12** 15282–90

[14] Ribeaucourt L, Savidand G, Lincot D and Chassaing E 2011 Electrochemical study of one-step electrodeposition of copper–indium–gallium alloys in acidic conditions as precursor layers for Cu(In, Ga)Se_2 thin film solar cells *Electrochim. Acta* **56** 6628–37

[15] Rampino S *et al* 2012 15% efficient Cu(In, Ga)Se_2 solar cells obtained by low-temperature pulsed electron deposition *Appl. Phys. Lett.* **101** 132107

[16] Panthani M G, Akhavan V, Goodfellow B, Schmidtke J P, Dunn L, Dodabalapur A, Barbara P F and Korgel B A 2008 Synthesis of $CuInS_2$, $CuInSe_2$, and $Cu(In_xGa_{1-x})Se_2$ (CIGS) nanocrystal 'inks' for printable photovoltaics *J. Am. Chem. Soc.* **130** 16770–7

[17] Guo Q, Ford G M, Hillhouse H W and Agrawal R 2009 Sulfide nanocrystal inks for dense $Cu(In_{1-x}Ga_x)(S_{1-y}Se_y)_2$ absorber films and their photovoltaic performance *Nano Lett.* **9** 3060–5

[18] Guo Q, Ford G M, Agrawal R and Hillhouse H W 2013 Ink formulation and low-temperature incorporation of sodium to yield 12% efficient Cu(In, Ga)(S, Se)$_2$ solar cells from sulfide nanocrystal inks *Prog. Photovolt. Res. Appl.* **21** 64–71

[19] Chang S, Chiang M, Chiang C, Yuan F, Chen C, Chiu B, Kao T, Lai C and Tuan H 2011 Facile colloidal synthesis of quinary $CuIn_{1-x}Ga_x(S_ySe_{1-y})_2$ (CIGSSe) nanocrystal inks with tunable band gaps for use in low-cost photovoltaics *Energ. Environ. Sci.* **4** 4929–32

[20] Hibberd C J, Chassaing E, Liu W, Mitzi D B, Lincot D and Tiwari A N 2010 Non-vacuum methods for formation of Cu(In, Ga)(Se, S)$_2$ thin film photovoltaic absorbers *Prog. Photovolt. Res. Appl.* **18** 434–52

[21] Wang G, Wang S, Cui Y and Pan D 2012 A novel and versatile strategy to prepare metal–organic molecular precursor solutions and its application in Cu(In, Ga)(S, Se)$_2$ solar cells *Chem. Mater.* **24** 3993–7

[22] Todorov T K, Gunawan O, Gokmen T and Mitzi D B 2013 Solution-processed Cu(In, Ga)(S, Se)$_2$ absorber yielding a 15.2% efficient solar cell *Prog. Photovolt. Res. Appl.* **21** 82–7

[23] Zuzhou X, Maojun Z, Sida L, Li M and Wenzhong S 2013 Silicon nanowire array/Cu_2O crystalline core–shell nanosystem for solar-driven photocatalytic water splitting *Nanotechnology* **24** 265402

[24] Jung Y C and Bhushan B 2009 Mechanically durable carbon nanotube–composite hierarchical structures with superhydrophobicity, self-cleaning, and low-drag *ACS Nano* **3** 4155–63

[25] Xiao J, Wan L, Yang S, Xiao F and Wang S 2014 Design hierarchical electrodes with highly conductive $NiCo_2S_4$ nanotube arrays grown on carbon fiber paper for high-performance pseudocapacitors *Nano Lett.* **14** 831–8

[26] Hu C, Yang D, Wang Z, Huang P, Wang X, di Chen, Cui D, Yang M and Jia N 2013 Bio-mimetically synthesized Ag@BSA microspheres as a novel electrochemical biosensing interface for sensitive detection of tumor cells *Biosens. Bioelectron.* **41** 656–62

[27] Chen G, Seo J, Yang C and Prasad P N 2013 Nanochemistry and nanomaterials for photovoltaics *Chem. Soc. Rev.* **42** 8304–38

[28] Li L, Chen S, Wang X, Bando Y and Golberg D 2012 Nanostructured solar cells harvesting multi-type energies *Energ. Environ. Sci.* **5** 6040–6

[29] Zhang G, Finefrock S, Liang D, Yadav G G, Yang H, Fang H and Wu Y 2011 Semiconductor nanostructure-based photovoltaic solar cells *Nanoscale* **3** 2430–43

[30] Byun J, Lee J I, Kwon S, Jeon G and Kim J K 2010 Highly ordered nanoporous alumina on conducting substrates with adhesion enhanced by surface modification: universal templates for ultrahigh-density arrays of nanorods *Adv. Mater.* **22** 2028–32

[31] Donglai G, Lixia F, Jianping S, Yifan L, Shengyou H and Xianwu Z 2007 Fabrication of a regular tripod Ni–P nanorod array and an AAO template with regular branched nanopores using a current-controlled branching method *Nanotechnology* **18** 405304

[32] Zhou T, Zheng M, Ma L, He Z, Li M, Li C and Shen W 2011 Size control of $CuInSe_2$ nanotube arrays via nanochannel-confined galvanic displacement *J. Mater. Chem.* **21** 17091–3

[33] Li M, Zheng M, Zhou T, Li C, Ma L and Shen W 2012 Fabrication and centeracterization of ordered $CuIn_{(1x)}Ga_xSe_2$ nanopore films via template-based electrodeposition *Nanoscale Res. Lett.* **7** 675

[34] Minwoo K A Y H 2013 Extended self-ordering regime in hard anodization and its application to make asymmetric AAO membranes for large pitch-distance nanostructures *Nanotechnology* **24** 505304

[35] Li Y, Ling Z Y, Chen S S and Wang J C 2008 Fabrication of novel porous anodic alumina membranes by two-step hard anodization *Nanotechnology* **19** 225604

[36] Yanbo L, Maojun Z, Li M and Wenzhong S 2006 Fabrication of highly ordered nanoporous alumina films by stable high-field anodization *Nanotechnology* **17** 5101

[37] He Z, Zheng M, Hao M, Zhou T, Ma L and Shen W 2011 Evolution process of orderly nanoporous alumina by constant high field anodization in oxalic acid electrolyte *Appl. Phys. A-Mater.* **104** 89–94